



Predicting the elasto-plastic response of short fiber reinforced composites using a computationally efficient multi-scale framework based on physical matrix properties

H. Ahmadi ^{a,b,*}, M. Hajikazemi ^{a,c}, W. Van Paepegem ^a

^a Department of Materials, Textiles and Chemical Engineering, Faculty of Engineering and Architecture, Ghent University, Technologiepark 46, Zwijnaarde, B-9052, Belgium

^b SIM M3 Program, Technologiepark 48, Zwijnaarde, B-9052, Belgium

^c Dutch Polymer Institute (DPI), P.O. Box 902, 5600 AX, Eindhoven, Netherlands

ARTICLE INFO

Keywords:

Short fiber reinforced composites
Anisotropic plasticity
Micromechanical analysis
Unit cell
Multi-step homogenization

ABSTRACT

Predicting the nonlinear mechanical response of short fiber reinforced composites (SFRCs) is a crucial and challenging task. In this paper, a computationally efficient multi-scale strategy is proposed to predict the anisotropic elasto-plastic behavior of SFRCs using the intrinsic mechanical behavior of the pure polymer and fibers without the requirements for reverse engineering. In doing so, different simple unit cells are first examined to find the one that can adequately describe the nonlinear mechanical response of SFRCs' representative volume elements (RVE) with aligned fibers. Considering the effects of packing configuration, fiber aspect ratio, volume fraction and material properties, the performance of different unit cells is investigated. Then, the homogenized mechanical responses of unit cells are linked to Hill's anisotropic plasticity model to correlate the mechanical response of the suggested unit cell to the continuum domain. Using the pseudo-grain approach and a numerical orientation averaging framework, the effects of fiber misalignment are taken into account. A multi-step homogenization strategy is also employed to consider the variation of fiber orientation tensor and volume fraction through the thickness. Finally, the validity and robustness of the proposed multi-scale strategy are extensively investigated based on the RVE-generated results and the available experimental observations.

1. Introduction

Nowadays, short fiber reinforced composites (SFRCs) are becoming one of the most widely used composite materials in the automotive industry due to their numerous advantages such as improved mechanical properties (compared to pure polymers), low manufacturing costs, high reproducibility and good design freedom for complex geometries [1–4]. Predicting the nonlinear mechanical response of SFRCs has a critical role in the design of composite structures. However, the prediction of the nonlinear behavior of SFRCs is a complex task since it largely depends on their microstructural information such as fiber length, fiber orientation and fiber volume fraction [5]. As a result, advanced models that can incorporate microstructural information and describe the nonlinear behavior of composite materials are in demand.

Among different analytical and numerical methods, Finite Element

Method (FEM) is a popular approach for predicting the mechanical response of materials in various length scales [6–8]. FEM has been frequently used to explore the mechanical behavior of SFRCs using micromechanical models (FEM modeling at micro-scale) [9–21]. To get insights into the mechanical behavior of the material under various loading conditions, this strategy relies on the representative volume elements (RVEs) and has the possibility to consider different sources of damage and nonlinearity for the materials. However, generating a realistic RVE for SFRCs is still a challenging task, especially when high fiber volume fractions/aspect ratios and fiber misalignments are required [20,22]. Besides, various microscopic investigations show variations of fiber volume fraction and orientation tensor across the thickness of SFRCs [5,23–25], increasing the complexity of modeling such microstructures [20]. Nevertheless, the main restriction of the RVE based FEM method is high computational costs for micromechanical

* Corresponding author. Department of Materials, Textiles and Chemical Engineering, Faculty of Engineering and Architecture, Ghent University, Technologiepark 46, Zwijnaarde, B-9052, Belgium.

E-mail address: hossein.ahmadi@ugent.be (H. Ahmadi).

analysis.

Adopting simplified unit cells with reasonable accuracy is of great interest to replace time-consuming RVE analysis. Unit cell based FEM analysis has many advantages such as simplicity, computational efficiency and the possibility of using a structured mesh for the analysis. Different researchers have employed unit cells with a single fiber to predict the mechanical response of SFRCs [11,26–30]. However, for such single fiber unit cells, the packing configuration has a significant influence on the mechanical response [26,28]. To overcome this drawback, linking the average strain field of single fiber unit cells to the mean-field homogenization (MFH) can be considered as a possible technique that approximately takes into account the interactions between the inclusions [31,32]. In general, such strategies lead to acceptable predictions of the nonlinear mechanical responses, however, the main limitations of this technique are the computational costs associated with the iteration process in the coupled FE-MFH model, as well as the lack of accuracy for SFRCs with high fiber volume fractions [31,32]. Only a few studies tried to use simplified multi-fiber unit cells for predicting the mechanical behavior of SFRCs [16,33]. However, there are no adequate investigations in the literature to shed light on this important topic and introduce a unit cell with good performance for the elasto-plastic response of SFRCs.

Although computational micromechanical methods are powerful techniques for simulating the nonlinear mechanical behaviors of SFRCs, they cannot be directly used for the structural-level analysis. For this reason, there is a requirement for multi-scale strategies that link the microstructural analysis to continuum models. A variety of plasticity models can be utilized to explore the anisotropic response of materials in the continuum domain [34–38]. In this regard, Hill's plasticity model has received much attention for addressing the anisotropic response of SFRCs [1,34,39]. Recent investigations in SFRCs have been focused on correlating the experimental data of coupon samples, for example in 0°, 90° and 45° with respect to the injection flow direction, to the Hill's potential function and advanced plasticity models [1,40,41]. It is shown that such strategy can predict the nonlinear response of SFRCs at the coupon level [1,40]. However, several experimental tests are needed which are time-consuming and costly. More importantly, there is not full control over the fiber orientations in injected molded samples so that even in 0°, 90° coupons, fibers are not all parallel. This leads to the condition that experimentally calibrated plasticity models depend on specific specimens and experiments. Thus, the microstructural information cannot be fully coupled with the plasticity model and there will be a requirement to perform experimental tests for any requested microstructure (material properties, volume fractions and average aspect ratio). On the other hand, from the analytical point of view, some effort was also made to link the calibrated mean-field homogenization (MFH) to Hill's plasticity model [42]. It was shown that Hill's plasticity criterion can fit very well the plasticity yield surfaces obtained from MFH for SFRCs. However, the evaluated parameters depend on the orientation tensors and a single Hill's model cannot be used for design purposes where fibers might be present in several orientations. It should be noted that the MFH provides fast and valuable predictions for the linear mechanical response of SFRCs. Nevertheless, their accuracy for the plastic regime, without reverse engineering of the polymer behavior, is still an open topic for SFRCs. Thus, it is important to focus on linking the numerical micromechanical approaches with advanced constitutive laws for predicting the anisotropic plasticity behavior of SFRCs.

One key step in predicting the mechanical behavior of SFRCs is considering the effects of fiber misalignments in the mechanical response of the material. The two-step homogenization methods have been extensively adopted to take into account the effects of fiber misalignment [43–47]. Although this technique has been mainly developed for MFH strategies [48,49], some interesting attempts have been made to link the numerical micromechanical models to two-step homogenization strategies [11,16,20,29,50]. However, there is still a requirement to use analytical solutions such as Voigt, Reuss,

Mori-Tanaka, Double-inclusions and self-consistent approaches for the orientation averaging technique to evaluate the macroscopic mechanical behavior of the materials. Moreover, it is not always an easy task to implement and link the advanced constitutive models to the analytical orientation averaging approaches, especially for the nonlinear mechanical behavior.

In the present study, a computationally efficient multi-scale framework is proposed to predict the elasto-plastic response of SFRCs under multi-axial loading conditions without reverse engineering of the polymer behavior. To do so, a multi-fiber unit cell based on the actual fiber/matrix material and geometrical properties is first introduced that reasonably captures the nonlinear mechanical response of completely aligned SFRCs' RVEs without the requirement to calibrate fibers' tip and side distances. Then, the mechanical response obtained from the unit cell is transferred to the continuum domain using an anisotropic plasticity model (Hill's plasticity). In this regard, the material parameters of the plasticity model are calibrated based on the stress-strain response obtained from the selected unit cell using an optimization approach. Next, the effects of fiber misalignments are addressed by implementing a fully numerical framework that does not have the limitation of analytical orientation averaging approaches. The employed strategy provides the possibility of introducing the variation of volume fraction and orientation tensor in the mechanical response of SFRCs based on multi-step homogenization.

The novel aspects of the current work can be summarized as follows:

- Suggesting a user-friendly multi-scale framework for predicting the anisotropic nonlinear response of SFRCs which correlate the nonlinear response with microstructural information using the intrinsic elasto-plastic behavior of pure polymer.
- Introducing a computationally efficient unit cell for predicting the elasto-plastic response of SFRCs
- Investigating the accuracy of different unit cells for estimating the elasto-plastic response of SFRCs considering the effects of packing configurations, aspect ratio, volume fraction and material properties
- Coupling the response of multi-fiber unit cells to the Hill's plasticity model for exploring the nonlinear response in the continuum domain.
- Replacing analytical orientation averaging approaches with numerical homogenization strategies and combining with anisotropic plasticity models for SFRCs.
- Implementing a multi-step homogenization strategy for considering the variation of fiber volume fraction and fiber orientation tensor through the thickness.

Combining the above novel modeling ingredients provides a computationally efficient multi-scale framework that predicts accurately the anisotropic nonlinear response of SFRCs correlated with microstructural information without the requirement for reverse engineering.

2. Methodology

2.1. Micromechanics

In this study, finite element modeling is performed to explore the nonlinear mechanical response of SFRCs under in-plane and out-of-plane loading conditions. In this regard, various types of unit cells (single fiber and multi-fiber) have been selected to predict the effective elasto-plastic response of aligned SFRCs. The main reason for selecting different shapes of the unit cell is that the fiber distribution in unit cells has important effects on the mechanical behavior of the unit cell. Indeed, the distribution of fibers in such microstructures can alter the local stress fields due to different interactions between the fibers. The schematic illustrations of these microstructures in the local coordinate system (1, 2 and 3) are presented in Fig. 1.

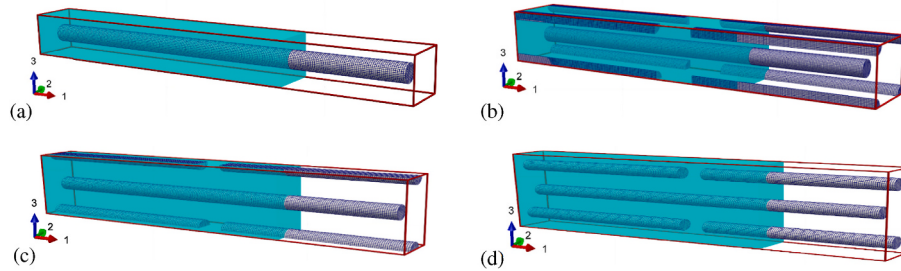


Fig. 1. Selected unit cells for predicting the mechanical response of SFRCs and the employed mesh with the fiber aspect ratio 20 and volume fraction 13% considering equal side and tip distance; (a) unit cell 1, (b) unit cell 2, (c) unit cell 3, (d) unit cell 4.

Fig. 2 demonstrates a schematic view of the fiber packing configurations in different employed unit cells.

It is noted that both side and tip distances are selected, respectively, as half of the vertical and horizontal distances between neighboring fibers in the periodic structure. Moreover, the tip and side distances should be selected in a way that matches the required volume fraction of the model. In this regard, one should define a relation between the tip and side distances (for example $w_{tip} = w_{side}$ or $w_{tip} = 2w_{side}$) so that both the tip and side distances will be dependent on the volume fraction and aspect ratio. Additionally, it is also possible to consider a fixed value for one of the tip or side distances and calculate the other distance by satisfying the volume fraction. In this study, the first strategy is employed for generating the geometry of each unit cell.

$$\frac{V_{Inclusion}}{V_{Unit\ cell}} - \text{fiber volume fraction} = 0, \quad (1)$$

where $V_{Inclusion}$ and $V_{Unit\ cell}$ are, respectively, the volume of the inclusions and unit cell where the fiber volume fraction is the given volume fraction of SFRCs for generating the model.

Periodic boundary conditions (PBCs) [51,52] are applied to link the displacement fields u between corresponding nodes at the opposite boundaries, which can be defined as [51]

$$u_j^{i+} - u_j^{i-} = \varepsilon_{ij} l_i \quad (i, j = x, y, z), \quad (2)$$

where ε_{ij} and l_i refer, respectively, to the macroscopic strain tensor and length of the model in i direction of the global coordinate system (x, y, z). The effective homogenized response of the microstructure (average stress (σ) and average strain (ε) responses) can be calculated for the whole microstructure volume (V) using the information at the integration points by

$$\sigma_{ij} = \frac{1}{V} \int_V \sigma_{ij} dV, \quad (3)$$

$$f(\sigma) = \sqrt{F(\sigma_{22} - \sigma_{33})^2 + G(\sigma_{33} - \sigma_{11})^2 + H(\sigma_{11} - \sigma_{22})^2 + 2L\sigma_{23}^2 + 2M\sigma_{31}^2 + 2N\sigma_{12}^2}, \quad (7)$$

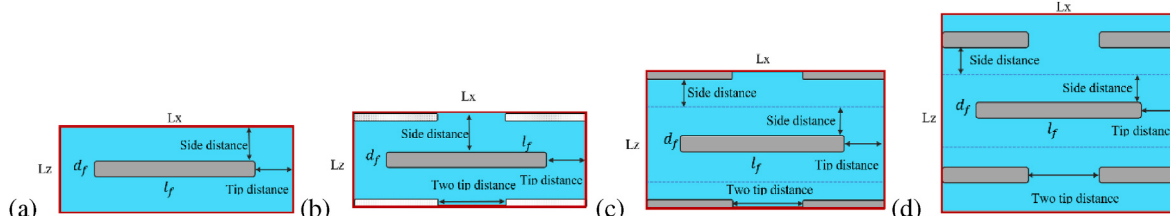


Fig. 2. Schematic representation of the fiber packing configuration in different unit cells with fully aligned SFRPs; (a) unit cell 1, (b) unit cell 2, (c) unit cell 3, (d) unit cell 4.

where σ_{ij} represent the components of the stress in the local coordinate system and the parameters of the Hill's plasticity model can be represented as

$$F = \frac{1}{2} \left(\frac{1}{R_{22}^2} + \frac{1}{R_{33}^2} - \frac{1}{R_{11}^2} \right), G = \frac{1}{2} \left(\frac{1}{R_{11}^2} + \frac{1}{R_{33}^2} - \frac{1}{R_{22}^2} \right), H = \frac{1}{2} \left(\frac{1}{R_{11}^2} + \frac{1}{R_{22}^2} - \frac{1}{R_{33}^2} \right), L = \frac{3}{2R_{23}^2}, M = \frac{3}{2R_{13}^2}, N = \frac{3}{2R_{12}^2} \quad (8)$$

Moreover, the parameters of yield stress ratios R_{ij} in various directions can be expressed in terms of yield stresses σ_{ij}^y as

$$R_{11} = \frac{\sigma_{11}^y}{\sigma_0}, R_{22} = \frac{\sigma_{22}^y}{\sigma_0}, R_{33} = \frac{\sigma_{33}^y}{\sigma_0}, R_{12} = \frac{\sigma_{12}^y}{\tau_0}, R_{13} = \frac{\sigma_{13}^y}{\tau_0}, R_{23} = \frac{\sigma_{23}^y}{\tau_0}, \quad (9)$$

where σ_0 is a reference yield stress and τ_0 is equal to $\tau_0 = \sigma_0 / \sqrt{3}$. It should be noted that the parameters of the yield stress ratios can be obtained using the mechanical response of microstructures under different loading conditions.

The plasticity flow rule for this model can be derived as

$$d\varepsilon_{pl} = d\lambda \frac{\partial f}{\partial \sigma} \begin{bmatrix} H(\sigma_{11} - \sigma_{22}) + G(\sigma_{11} - \sigma_{33}) \\ F(\sigma_{22} - \sigma_{33}) + H(\sigma_{22} - \sigma_{11}) \\ G(\sigma_{33} - \sigma_{11}) + F(\sigma_{33} - \sigma_{22}) \\ 2N\sigma_{12} \\ 2M\sigma_{31} \\ 2L\sigma_{23} \end{bmatrix}, \quad (10)$$

where $d\varepsilon_{pl}$ and $d\lambda$ are the vector of the plastic strain increments and the scalar plastic multiplier, respectively. Different hardening functions can be used to represent the nonlinear response in the plastic regime. The exponential-linear law is chosen here to describe the hardening response

in the plastic region, as follows

$$R(\bar{\varepsilon}_{pl}) = k_1(\bar{\varepsilon}_{pl}) + k_2(1 - \exp(-m\bar{\varepsilon}_{pl})), \quad (11)$$

where k_1 , k_2 and m are the parameters of the hardening function, while $\bar{\varepsilon}_{pl}$ is the equivalent plastic strain. In commercial finite element software, the elastic constants and Hill's plasticity parameters can be defined directly, while the hardening function needs to be converted to tabular inputs.

In order to identify the material parameters for the assumed plasticity model as well as the hardening function, different curve fitting and optimization strategies can be used. In this study, the Nelder-Mead optimization technique [51] with a single-element FE test is adopted to extract the parameters based on multiple stress-strain curves obtained from unit cell analysis (see Fig. 3). Alternatively, it is also possible to fit the hardening function based on a single stress-strain curve under a specific uniaxial loading condition using the least-squares method and then evaluate the Hill's plasticity yield stress ratios R_{ij} based on the stress-strain curves in other loading directions. However, the accuracy of this approach will be less than the optimization framework where stress-strain curves for multiple loading directions are used together, for calibration of Hill's model.

2.3. Orientation averaging and multi-step homogenizations

As mentioned, fiber orientations play an important role in the mechanical behavior of short fiber composites. In the three-dimensional domain, the orientation of a single fiber can be introduced using a unit vector \mathbf{p} based on the in-plane (φ) and out-of-plane (θ) orientations (see Fig. 4) which is written as

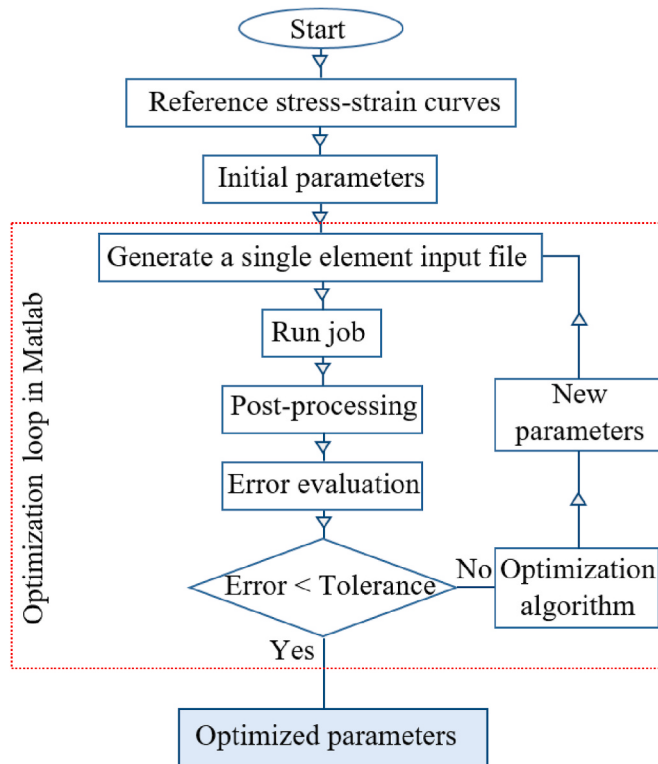


Fig. 3. Flowchart illustrating the parameter identification steps for the material constants of the plasticity model.

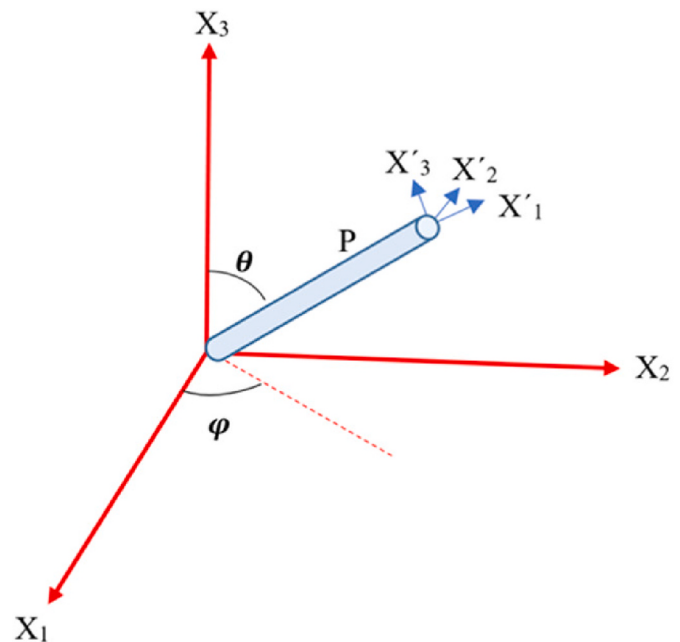


Fig. 4. Illustration of the orientation of a single fiber in the spherical coordinates system.

$$\mathbf{p} = \begin{bmatrix} \sin \theta \cos \varphi \\ \sin \theta \sin \varphi \\ \cos \theta \end{bmatrix} \quad (12)$$

Fig. 4 demonstrates the schematic view of the orientation of a single fiber in the global spherical coordinates system (X_1 , X_2 and X_3), while the local coordinate system is represented by (X'_1 , X'_2 and X'_3).

The orientation distribution function $\psi(\mathbf{p})$ provides essential information about the probability of finding fibers in any given orientation between (θ, φ) and $(\theta + d\theta, \varphi + d\varphi)$ and it should satisfy the following conditions [53]:

$$\oint \psi(\mathbf{p}) \sin \theta d\varphi d\theta = 1, \quad (13)$$

$$\psi(\mathbf{p}) = \psi(-\mathbf{p}) \quad (14)$$

Therefore, the second-order (**a**) and fourth-order (**A**) orientation tensors can be calculated using the following averaging procedure [53]:

$$a_{ij} = \oint p_i p_j \psi(\mathbf{p}) d\mathbf{p}, \quad (15)$$

$$a_{ijkl} = \oint p_i p_j p_k p_l \psi(\mathbf{p}) d\mathbf{p} \quad (16)$$

$$d\mathbf{p} = \sin \theta d\varphi d\theta \quad (17)$$

The two-step homogenization approach is widely used to compute the mechanical response of composite materials with complex microstructures [11,20,43,48,50,54–56]. This technique decomposes the microstructure into several pseudo-grains where each grain has microstructures with consistent physical properties (same orientation, same aspect ratio, etc.). To evaluate the effective mechanical behavior of the composite, this approach requires two homogenization steps. The first step is to homogenize the response of each grain, which can be obtained using MFH or finite element modeling. The second step is to obtain the total stiffness for all grains, which can be computed using analytical approaches (for example Voigt, Reuss, Mori-Tanaka, Double-inclusions and self-consistent approaches).

In the present study, a numerical multi-step homogenization strategy with an orientation averaging approach is adopted that accurately considers the effects of fiber misalignments and core/shell thicknesses. In this regard, the pseudo-grain approach is employed to decompose the microstructure into several groups where the homogenized response of

each grain is specified to a layer in parallel and series laminates. In this case, the thickness of each ply t_i represents the weight w_i of each grain where the orientation of each ply is defined based on the orientation of each grain. Then, Hill's plasticity model or any other anisotropic model for an aligned unit cell can be used to describe the nonlinear mechanical behavior of the material. Thus, the homogenization steps can be performed directly in finite element modeling without the requirement for an approximate analytical framework (see **Fig. 5**). After obtaining the effective mechanical response for the misaligned structure, the parameters of the Hill's model can be re-evaluated for the new structure to represent the mechanical response of composite material with misaligned fiber. The same procedure can be applied to the core/shell structure. It should be noted that since the homogenized response is used in this multi-step homogenization, only limited computational costs will be needed. Moreover, for industrial applications, some fitted functions can be used to represent Hill's parameters based on the eigenvalue of the orientation tensor. In this case, there will be no requirement for orientation averaging during the structural analysis of complex geometries.

3. Results and discussions

3.1. Micromechanics of aligned SFRCs

In this section, the performance of different unit cells is investigated and compared with RVE-generated results to indicate the possibility of estimating the nonlinear mechanical response of aligned SFRCs' RVE using simplified unit cells. In this regard, a SFRP RVE made of glass/polyamide is selected as the reference to evaluate the nonlinear response of SFRCs under different loading conditions. The aspect ratio and volume fraction of the glass fibers are defined, respectively, as $A_r = 20$ and $V_f = 0.13$ where the elastic properties are given as follows [28]:

$$E_f = 72000 \text{ MPa}, v_f = 0.22, E_m = 2100 \text{ MPa} \text{ and } v_m = 0.3,$$

where E and v are, respectively, Young's modulus and the Poisson's ratio while subscript f and m refer to the fiber and matrix, respectively. The material properties of the polymer are assumed to be elasto-perfectly plastic with the yield stress $\sigma_y = 50 \text{ MPa}$ and the interface between the fibers and matrix is considered to be perfectly bounded. The main reason for selecting such simplified plastic behavior for the pure polymer is to focus on the modeling ingredients as a whole rather than detailing each step of the multi-scale framework. It is clear that the approach can incorporate any plasticity behavior for the polymer. This

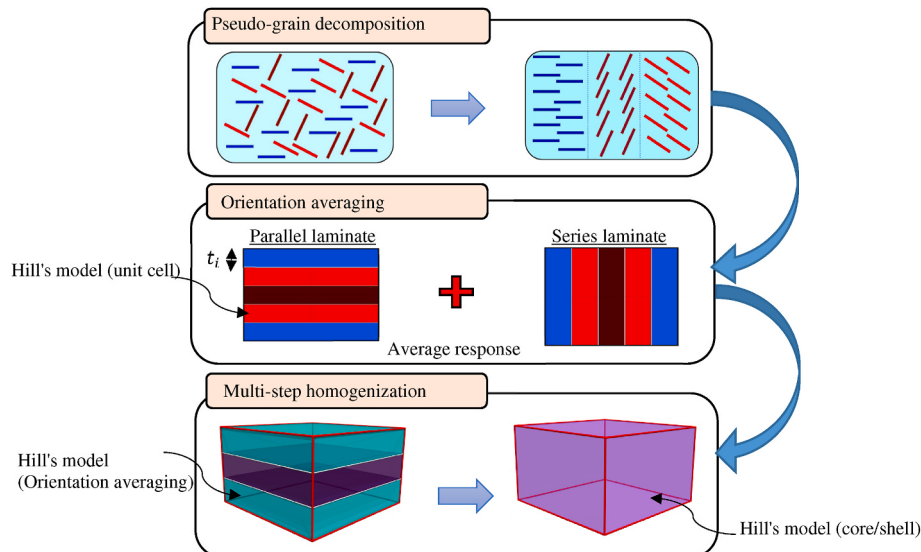


Fig. 5. Schematic demonstration of utilized orientation averaging approach and multi-step homogenization based pseudo-grain approach.

selection of the plastic behavior is also consistent with the available literature and provides easy-to-use reference data for different analytical studies where the elastic response can be distinguished from the plastic response (for example in the mean-field homogenization). To model the plastic behavior of the pure polymer at the microstructure level, the von Mises plasticity model is adopted. On the other hand, the Digimat software is employed to generate the geometry of all RVEs for predicting the mechanical response of SFRCs. The RVE generation process is based on random fiber placement where the minimum relative distance between inclusions is specified as 0.05, normalized by the fiber diameter. The model is then linked to a commercial finite element software for meshing and applying loading/boundary conditions. Homogenizations are carried out using an in-house Python script, in order to calculate the average stress-strain response of SFRCs. On the other hand, the unit cells are generated directly in the commercial finite element program using Python scripts developed by the authors. It should be noted that due to the complexity of SFRCs' microstructural geometry, the RVE generation algorithm based on random fiber placement has some limitations for RVEs with high volume fractions and fiber misalignments depending on the selected input parameters (fiber geometry, aspect ratio, volume fraction and orientation tensor).

The 10-noded tetrahedral element (C3D10) is used to discretize the generated RVEs, while a very fine mesh has been employed to capture the stress fields in the high-stress zones of the SFRCs. Additionally, after a mesh sensitivity analysis, more than 675,000 elements are utilized to measure the mechanical response of the materials under various loading conditions. The size of RVEs are selected as $(0.7\text{mm} \times 0.07\text{mm} \times 0.07\text{mm})$ and $(0.6\text{mm} \times 0.1\text{mm} \times 0.1\text{mm})$ for the RVE1 and RVE2, respectively. Fig. 6 depicts the geometry of the employed RVEs and the corresponding meshes to predict the nonlinear mechanical response of aligned SFRP. It should be noted that the length and diameter of the cylindrical fibers are defined, respectively, as $l_f = 200\mu\text{m}$ and $d_f = 10\mu\text{m}$. Since the number of fibers and the size of RVEs are important parameters for predicting the nonlinear mechanical response of SFRCs, only the converged results are reported in this study. In order to have consistency in comparison between the performance of various unit cells, similar tip and side distances ($w_{\text{tip}} = w_{\text{side}}$) are defined for generating the unit cells. Fig. 7 demonstrates the effective mechanical response of selected unit cells and RVEs under various longitudinal and transverse loading conditions. Scrutinizing the obtained results depicts that there is a good agreement between the stress-strain responses of different unit cells and RVEs at the early stages of loading. However, by applying further loads, some discrepancies can be observed in the nonlinear mechanical response of the unit cells which are subjected to the axial tensile load. The main reasons for having such discrepancies are the effects of fiber interactions which are differently considered in each unit cell. It can be clearly seen that unit cell 1 and unit cell 2, respectively, exhibit the lower and upper bounds of the nonlinear mechanical response for the SFRCs' RVEs under the longitudinal tensile load. Furthermore, the unit cell 4 represents the best prediction for this loading condition. The matrix plasticity in unit cell 1 begins at the areas near the fiber tips which expands to surrounding

areas encompassed by the matrix. By applying further loads, the plasticity extends toward the areas near the center of the fiber. For the unit cell 1, there are no close fibers at the end of the fiber that can transfer the stresses further in the longitudinal direction. On the other hand, in the multi-fiber unit cells, there are interactions of fibers so that the released matrix stress due to the plasticity can be better transferred in the model. In these unit cells, the matrix plasticity also starts at the areas near the tip of the fibers, however, its expansion to the material is controlled by other neighboring fibers as well. Therefore, considering the interaction of the fibers in unit cells 2, 3 and 4 has led them to model a material behavior which is much closer to that of a multi-fiber RVE with random fiber packing configuration. It should be noted that due to the periodicity of the selected unit cells, unit cell 3 leads to a more uniform packing configuration than unit cell 4. It should be also highlighted that there are no significant differences in the effective mechanical response of unit cells and RVEs in other loading conditions. A possible explanation is that imposing such loading conditions leads to fewer stress concentrations in the microstructural response compared to the longitudinal tensile load.

The effects of packing configuration are also investigated for the employed unit cells to address the dependency of their mechanical response to different tip-side distances. The outcomes of two different packing configurations ($w_{\text{tip}} = w_{\text{side}}$ and $w_{\text{tip}} = 2w_{\text{side}}$) are presented in Fig. 8. It can be seen that only the stress-strain response of the single fiber unit cell (unit cell 1) is highly affected by the tip-side distances. However, the multi-fiber unit cells show very little dependency on the packing configuration due to the presence of surrounding fibers. It should be noted that the fiber volume fraction was kept constant for different packing configurations and only the side and tip distances were changed. It is also noteworthy to mention that the value of the tip distance could be decreased to find a better prediction for the mechanical response of a single fiber unit cell. However, the reference data of multi-fiber RVEs would be needed to confirm the accuracy of the model.

Using the same material properties with the fiber volume fraction 20%, the influence of different fiber aspect ratios is explored to illustrate the capability of different unit cells to predict the nonlinear mechanical response of SFRCs with different aspect ratios in higher volume fractions. The tensile stress-strain response of SFRCs with two distinct aspect ratios is shown in Fig. 9. In summary, the results depict that increasing the aspect ratio of the fibers improves the mechanical response of the SFRCs, and unit cell 4 can approximately predict the nonlinear mechanical response for a typical range of aspect ratios.

Additionally, in order to investigate the limitation of the employed unit cell for predicting the mechanical response of SFRCs with high fiber volume fractions, fully aligned SFRP samples with 30% fiber volume fraction and $A_r = 20$, are selected. Moreover, the mechanical properties of both the fiber and matrix are considered to be the same as the previous cases. The size of RVEs is considered as $(0.5\text{ mm} \times 0.06\text{ mm} \times 0.06\text{ mm})$ and $(0.5\text{ mm} \times 0.075\text{ mm} \times 0.075\text{ mm})$ for RVE 1 and RVE 2, respectively. For each RVE size, several fully aligned RVE models are generated to have a better understanding of the effects of fiber packing configuration for high fiber volume fraction samples. Fig. 10 demonstrates the stress-strain response of the material under longitudinal and

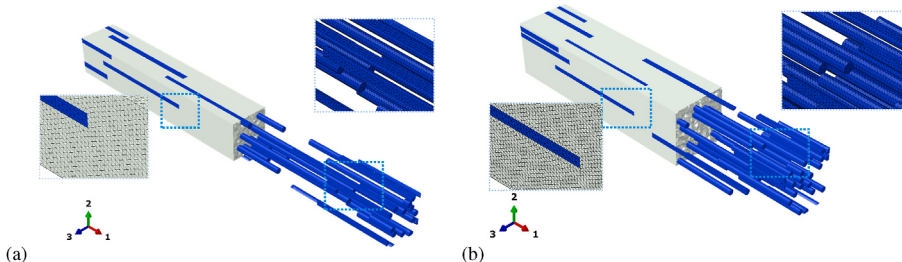


Fig. 6. Demonstration of selected glass/polyamide RVEs with the fiber aspect ratio 20 and volume fraction 13%; (a) RVE 1 with 28 fibers and 675,033 elements(b) RVE 2 with 49 fibers and 1,105,941 elements.

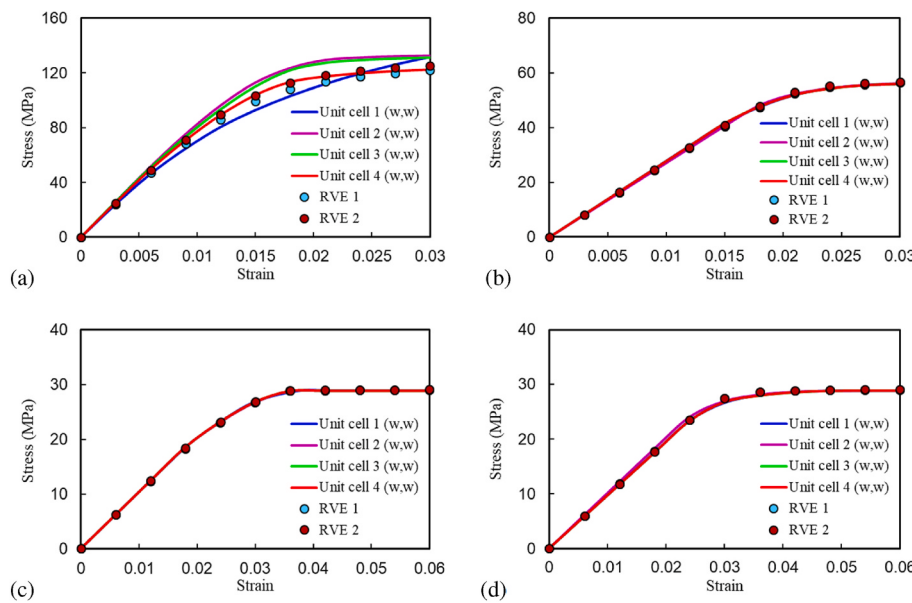


Fig. 7. The stress-strain response of glass SFRCs with the fiber aspect ratio 20 and volume fraction 13%; (a) longitudinal tensile load, (b) transverse tensile load, (c) longitudinal pure shear load, (d) transverse pure shear load.

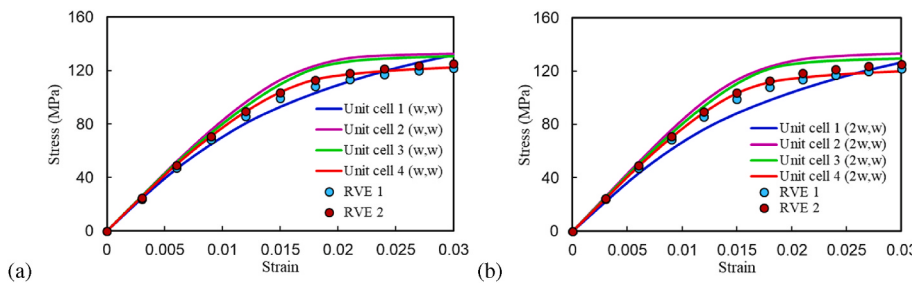


Fig. 8. Effects of packing configurations in the stress-strain response for longitudinal tension of glass/polyamide SFRCs with the fiber aspect ratio 20 and fiber volume fraction 13%; (a) tip and side distances (w, w), (b) tip and side distances (2w, w).

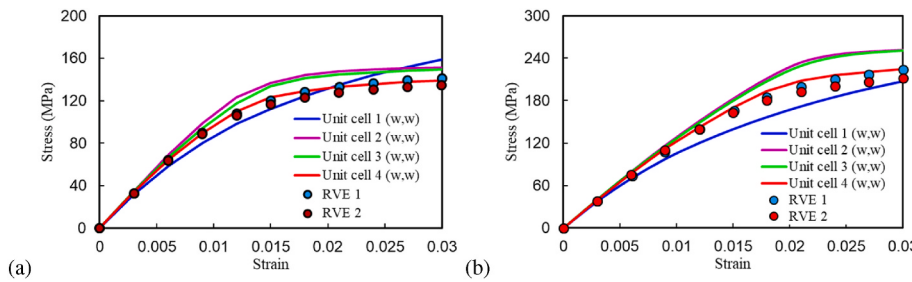


Fig. 9. The tensile stress-strain response of glass/polyamide SFRCs in the longitudinal direction with the fiber volume fraction 20% and different fiber aspect ratios; (a) aspect ratio of 15, (b) aspect ratio of 30.

transverse tensile loads. Unlike the mechanical response in samples with lower fiber volume fractions, the results indicate that for the longitudinal loading condition the effect of the packing configuration is more highlighted for high fiber volume fractions. The comparison between the results reveals that a discrepancy can be even seen between the results of RVEs with similar sizes. The main reason is that increasing the fiber volume fraction, reduces the distance between the fibers so that the interaction between the fibers increases. It should be noted that due to a very small tip distance (less than $0.5d_f$), the unit cell 4 with equal tip and side distances shows a higher stress-strain response compare to the RVE data, corresponding to a highly packed geometry. However, by increasing the tip distance and reducing the side distance the results

show a better agreement with the RVE-generated results. Therefore, it is suggested to use the higher tip-to-side distance (for example as $2w$, $3w$) for the cases with high fiber volume fractions ($v_f > 0.2$) to ensure that the tip distance is large enough for transferring the stress and avoiding the high interactions due to very low tip distances.

Further investigations are conducted to analyze the possibility of estimating the nonlinear response of SFRCs with specific yield stress and hardening function. For this reason, the exponential-linear hardening function is considered to represent the hardening response of the pure polymer. The elastic behavior remains the same, while the following parameters are selected to describe the plastic response of the polymer: $\sigma_y = 29 \text{ MPa}$, $k_1 = 139.0 \text{ MPa}$, $k_2 = 32.7 \text{ MPa}$ and $m = 319.4$ [57]. A

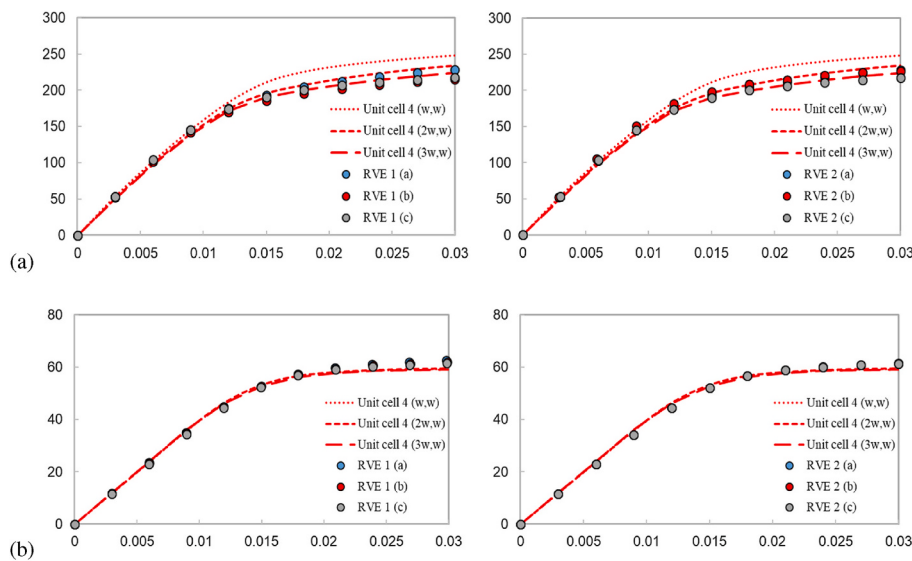


Fig. 10. The tensile stress-strain response of glass/polyamide SFRCs with the aspect ratio of $A_r = 20$ and volume fraction of 30% under; (a) longitudinal tensile load, (b) transverse tensile load.

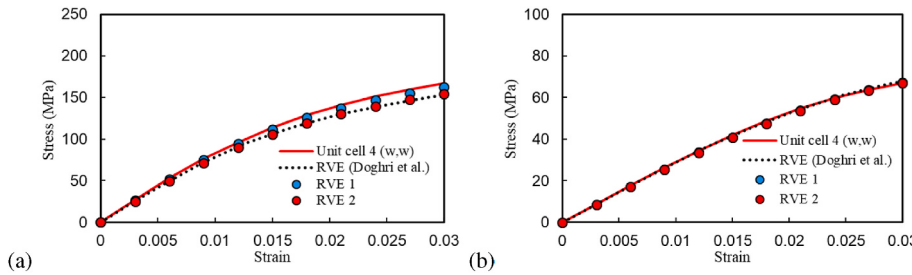


Fig. 11. The tensile stress-strain response of glass/polyamide SFRCs with the aspect ratio of $A_r = 15$ and volume fraction of 15.7% under; (a) longitudinal tensile load, (b) transverse tensile load.

unit cell of aligned SFRP with the aspect ratio $A_r = 15$ and volume fraction 15.7% is generated to compare the mechanical response with some reference data from the literature [57]. Fig. 11 presents the corresponding stress-strain response of different microstructures under longitudinal and transverse tensile loads. As it can be seen, some slight differences may be observed in the mechanical response of different RVEs under the longitudinal loads. However, the unit cell 4 shows acceptable performance for capturing the mechanical response of aligned SFRCs under different loading conditions.

3.2. Multi-scale modeling

In this section, the micromechanical response of SFRCs is correlated to an anisotropic constitutive law for representing the nonlinear mechanical response of the composite in the continuum domain. For this purpose, the effective behavior obtained from FE analysis of the unit cell (unit cell 4) is employed to evaluate the elastic constants and the material parameters of the plasticity model. First, the elastic properties of the SFRCs are determined using the linear mechanical response of SFRCs. Then, by performing the optimization framework, the material parameters of the plasticity model are computed based on the evaluated

nonlinear stress-strain curves of the unit cell 4 in different loading directions (two tension (longitudinal and transverse) and two pure shear loads (longitudinal and transverse)). The longitudinal pure shear strain is applied in the xy and yx planes while the transverse pure shear load is applied in the yz and zy planes. The calibrated parameters for the glass/polyamide SFRCs with $Ar = 20$ and 13% fiber volume fraction considering elasto-perfectly plastic behavior for the polymer (yield stress of $\sigma_y = 50 \text{ MPa}$) are given in Table 1. It is obvious in Fig. 12 that the micro-mechanical response of the SFRP is successfully predicted by the continuum model and the employed approach is able to efficiently describe the nonlinear mechanical response of SFRP for the imposed loading conditions.

In order to depict the capability of the calibrated Hill's model in predicting the nonlinear mechanical response of SFRCs in various orientations, aligned RVEs with different angles are generated. Fig. 13 shows the employed geometry and mesh for the selected RVEs with different orientations. The comparison between the axial stress-strain response of the suggested continuum model and the reference data is presented in Fig. 14. Comparison of the results confirms that the employed constitutive model is capable of capturing the nonlinear mechanical response of SFRCs in different orientations. It is noteworthy

Table 1

Evaluated parameters for the constitutive law of glass/polyamide SFRCs with an aspect ratio of 20 and volume fraction of 13%.

Parameters	E_1 (G Pa)	E_2 (G Pa)	ν_{12} (-)	ν_{23} (-)	G_{12} (G Pa)	G_{23} (G Pa)	R_{11} (-)	R_{22} (-)	R_{12} (-)	R_{23} (-)	σ_0 (MPa)	k_1 (MPa)	k_2 (MPa)	m (-)
Values	8.47	2.78	0.283	0.373	1.035	0.971	0.9511	0.4981	0.430	0.440	53.29	753.42	62.49	999.54

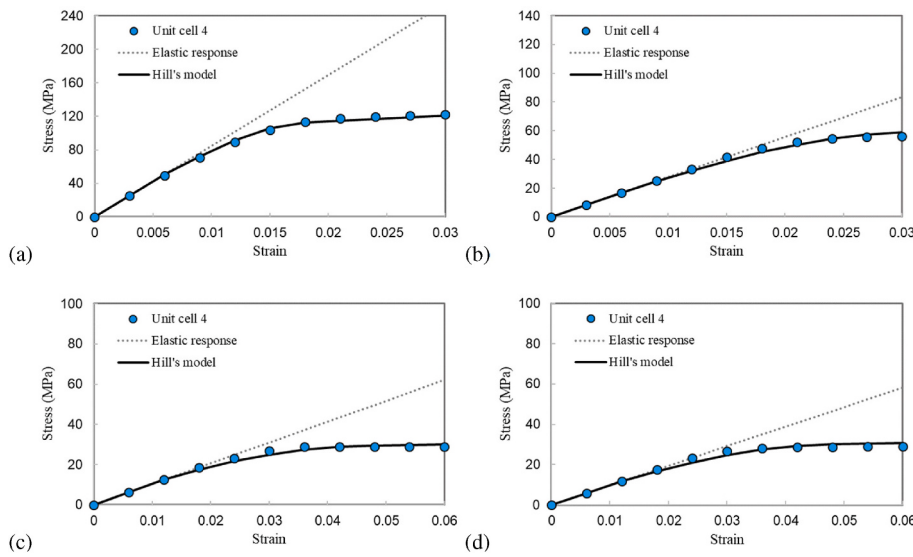


Fig. 12. Comparison between the stress-strain response of the microstructural analysis and Hill's plasticity model for glass/polyamide SFRP with the aspect ratio of 20 and the volume fraction of 13%; (a) longitudinal tensile load, (b) transverse tensile load, (c) longitudinal pure shear load, (d) transverse pure shear load.

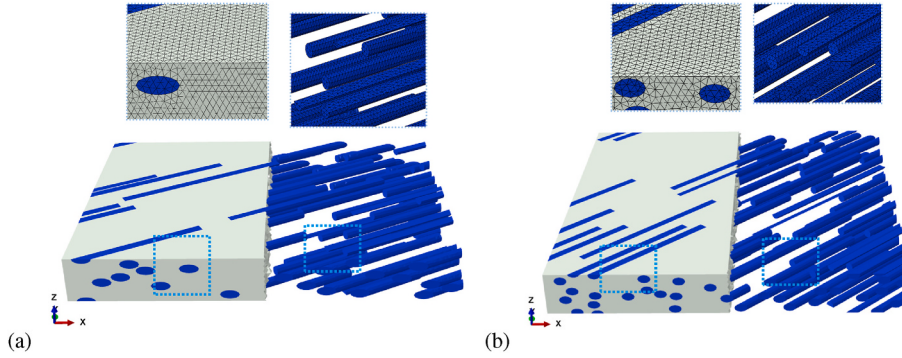


Fig. 13. Demonstration of selected glass/polyamide RVEs with the aspect ratio of 20 and volume fraction of 13% with different orientations; (a) 30°, (b) 45°.

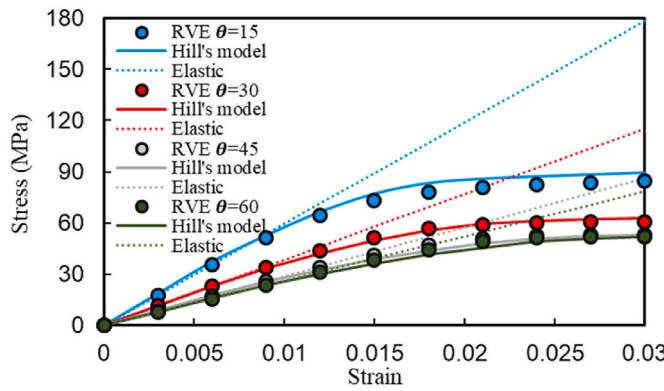


Fig. 14. The off-axis tensile stress-strain response of glass/polyamide SFRCs with a volume fraction of 13% and aspect ratios of 20 in different orientations.

that this verification could also be done by some biaxial loads imposed on the multi-fiber unit cell. Moreover, the parameter identification can be enhanced by adding more reference data in the material identification stage. For example, considering the low computational cost of the proposed unit cell, it is possible to apply loading conditions corresponding to the orientation of 15 and 45° to the generated unit cell and add the data in the material identification stage to increase the accuracy

of the obtained parameters. It should be noted that in order to check the mechanical response for other orientations, the material coordinate system of the continuum model (Hill's model) is rotated.

As previously discussed, fiber misalignments have important influences on the mechanical response of SFRCs. Moreover, the significance of the utilized plasticity model becomes clear when it is used to estimate the mechanical response of complex microstructures. For this reason, the numerical orientation averaging framework presented in the preceding section is applied to estimate the nonlinear mechanical response of SFRCs with misaligned fibers. To have reference data for the suggested model, different RVEs with varying fiber orientations are simulated. The Digimat software [58] is used to model the geometry of RVEs, while the PBCs and the homogenization are performed using Python scripts in commercial finite element software (see Fig. 15). It should be noted that the orientation of each fiber can be directly extracted from the generated RVE and used in the orientation averaging procedure. In case just the second-order orientation tensor is provided, the orientation distribution function should be reconstructed using some approximate analytical solutions [53,59]. Fig. 16 presents the stress-strain response for different microstructures under the tensile loading condition. As shown in this figure, the obtained results are in good accordance with the RVE-generated data and the mechanical response of SFRCs is highly dependent on the selected microstructure.

To further assess the validity of the proposed strategy in predicting the nonlinear mechanical response of SFRCs, a microstructure having 3D fiber misalignment is selected. Fig. 17 indicates the generated RVE and

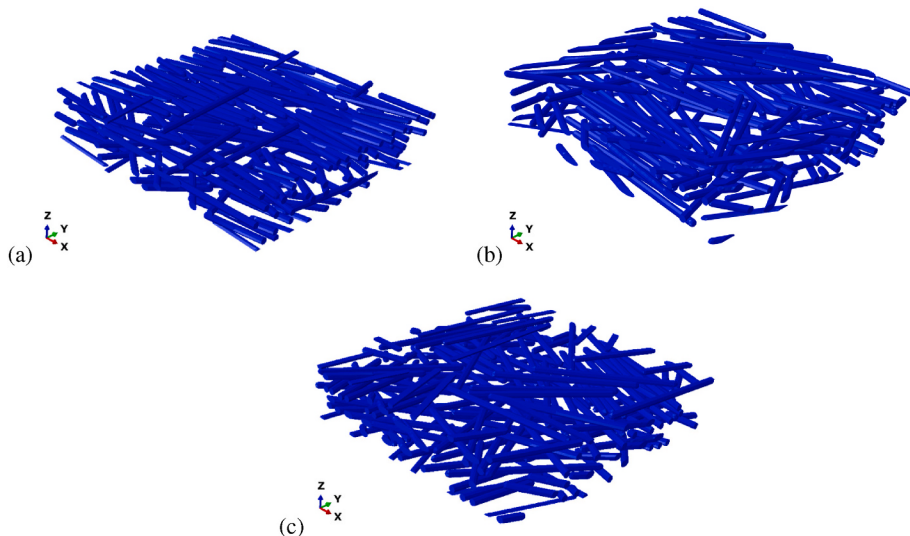


Fig. 15. Demonstration of selected glass/polyamide RVEs with the aspect ratio of 20 and the volume fraction of 13% with different fiber misalignment; (a) ($a_{11} = 0.81$, $a_{22} = 0.19$, $a_{12} = 0.05$), (b) ($a_{11} = 0.69$, $a_{22} = 0.31$, $a_{12} = 0.01$), (c) ($a_{11} = 0.51$, $a_{22} = 0.49$, $a_{12} = 0.01$).

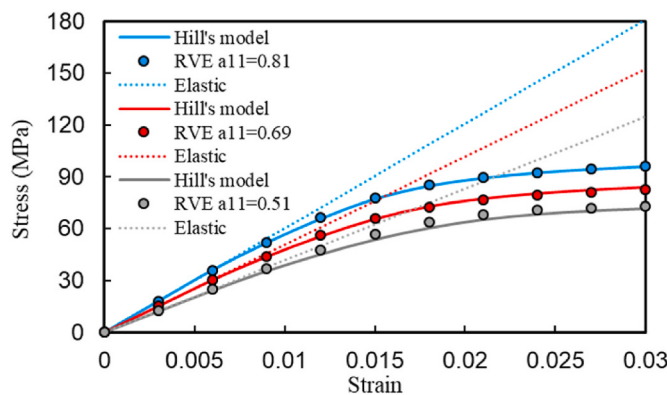


Fig. 16. The tensile stress-strain response of glass/polyamide SFRCs with a volume fraction of 13% and aspect ratios of 20 with different in-plane fiber misalignment.

the corresponding mesh with 228 fibers. Again, using the same orientation averaging approach, acceptable agreements are exhibited to predict the nonlinear mechanical response of SFRCs with complex fiber orientations (see Fig. 18).

After verifying the precision of the orientation averaging technique

used to evaluate the nonlinear mechanical response of SFRCs with complex microstructures, it is important to investigate the performance of the multi-step homogenization in predicting the mechanical response of SFRCs with core/shell layers. In doing so, a glass/polyamide SFRP with the stacking sequence of [0, 90, 0] is chosen. Due to the

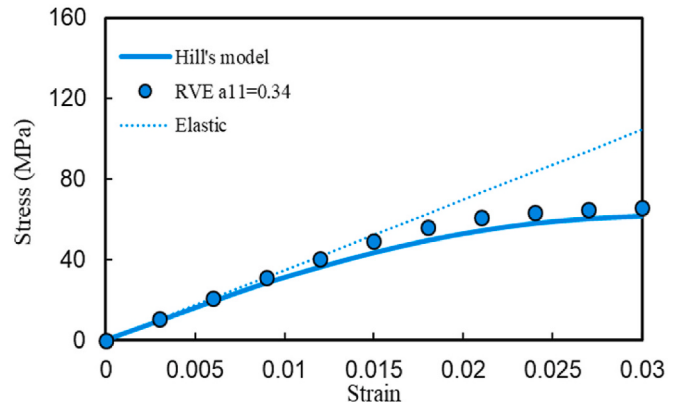


Fig. 18. The tensile stress-strain response of glass/polyamide SFRCs with the volume fraction of 13% and aspect ratios of 20 with 3D fiber misalignment.

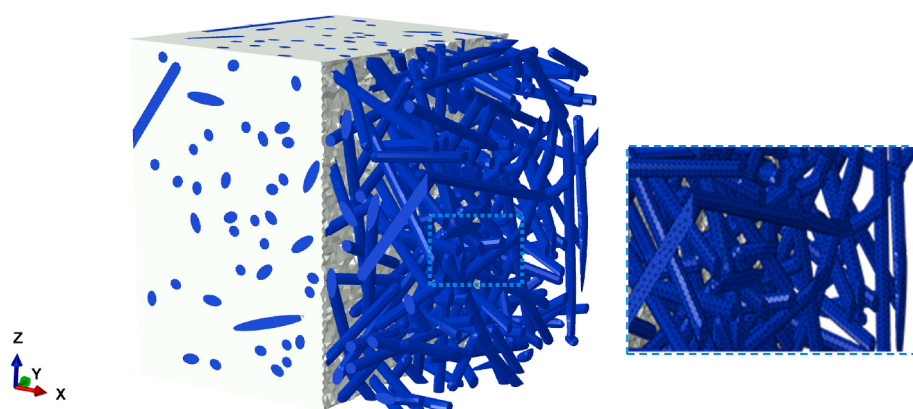


Fig. 17. Demonstration of selected glass/polyamide RVEs with the aspect ratio of 20 and volume fraction of 13% with 3D fiber misalignment ($a_{11} = 0.34$, $a_{22} = 0.35$, $a_{33} = 0.31$, $a_{12} = 0.01$, $a_{13} = 0.01$, $a_{23} = 0.01$).

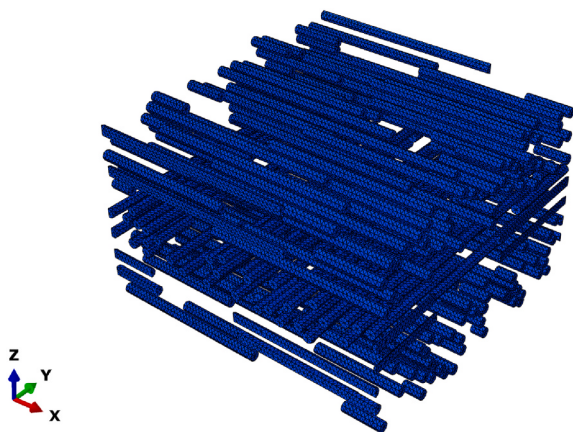


Fig. 19. Demonstration of multi-layer glass/polyamide RVEs with the aspect ratio of 20 and volume fraction of 13%.

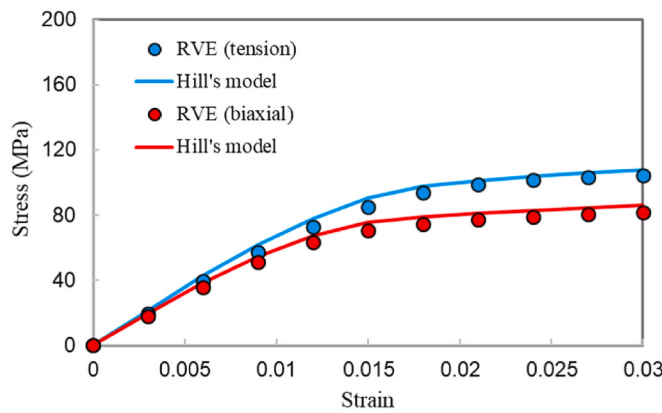


Fig. 20. The stress-strain response of multi-layer glass/polyamide SFRCs with a volume fraction of 13% and aspect ratios of 20 under tensile and biaxial (tension-compression) loading conditions.

computational limitation for analyzing the RVE, small ply thicknesses such as 0.08 mm and 0.05 mm are considered for the core and shell layers, respectively. Fig. 19 reveals the geometry and mesh of the selected multi-layer microstructure with 13% volume fraction. The mechanical responses of microstructure under tensile (x) and biaxial (tension(x)-compression(y)) is reported in Fig. 20. The comparison between the RVE-generated results and the utilized anisotropic model confirms the efficiency of the suggested methodology for predicting the mechanical response of SFRCs with complex microstructures under multi-axial loading conditions.

Finally, to demonstrate the applicability and performance of the proposed multi-scale strategy, the results of the suggested approach are compared with the data obtained from an available experimental

observation [24] where important information about the microstructural details is also provided. To this end, glass/polyamide-6 SFRCs with two different fiber volume fractions (6.4% and 15.2%) and aspect ratios (31.85 and 29.05) are selected, respectively [24]. The material properties of both fiber and matrix are assumed to be isotropic and defined as: $E_f = 72000 \text{ MPa}$, $\nu_f = 0.22$, $E_m = 3106 \text{ MPa}$ and $\nu_m = 0.38$. The plastic behavior of the matrix is extracted directly from the measured stress-strain response of the pure polymer and is used in a tabular form in the finite element modeling. It is noted that in the mentioned study [24], the mechanical response of the pure polymer was reported to be slightly dependent on the loading direction. In the current modeling, the mechanical behavior of the pure polymer in the injection direction is used to approximate the mechanical response of SFRPs in $\theta = 0$ and $\theta = 30$ (measured clockwise with respect to the injection molding direction) directions. The average orientation tensors [24] ((0.507, 0.473, 0.020) and (0.604, 0.354, 0.042)) are utilized to reconstruct the orientation of the fibers for the orientation averaging procedure and the RVEs generation. To add more benchmarking results, RVEs with 70 fibers are also simulated (see Fig. 21). Due to the difficulty in RVE generation for the specified fiber length and volume fraction, small differences can be seen in the orientation tensor of the RVE and the experimental data. Moreover, for the multi-scale modeling, six different loading conditions (two tension (longitudinal and transverse), two loads (corresponding to 15 and 45° orientation) and two pure shear loads (longitudinal and transverse) are imposed on the proposed unit cell to ensure the accuracy of the optimized parameters for the plasticity model.

Fig. 22 shows the obtained tensile stress-strain response in two different directions under 3% tensile strain. The results depict that there is a good agreement between the data evaluated using the proposed multi-scale strategy and the experimental results using intrinsic material properties of the constituents without a need for reverse engineering for the polymer behavior. Moreover, there is very good agreement between the results of the current multi-scale approach and those obtained by the cumbersome RVE analysis. The small discrepancy between the RVE results and the current approach for the sample with 30-degree can be explained by the small difference in the generated orientation tensors as well as the assumed geometries for the whole microstructure.

4. Conclusion

A multi-scale approach was suggested to efficiently predict the anisotropic elasto-plastic behavior of SFRCs considering the physical properties of the material without the requirement for reverse engineering. In this regard, different simplified unit cells were employed to evaluate the nonlinear mechanical response of SFRCs in a computationally efficient manner. It was shown that the selected simple multi-fiber unit cell can provide a good prediction for the nonlinear mechanical response of aligned SFRCs without the requirement for generating and analyzing complex and time-consuming RVEs. The results indicated that the tensile mechanical response of a single fiber unit cell is highly dependent on the selected packing configuration. On the other hand, Hill's plasticity model was considered to represent the

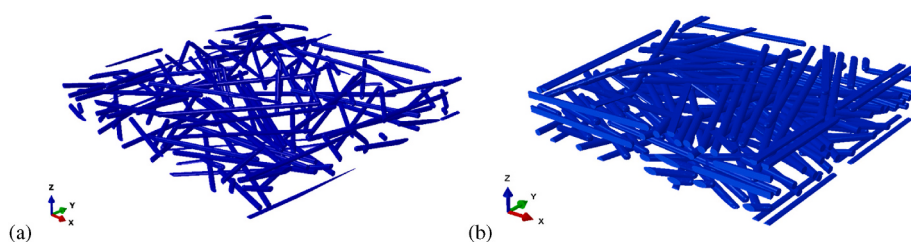


Fig. 21. Demonstration of selected glass/polyamide-6 RVEs with different geometries; (a) fiber aspect ratio of 31.85 and volume fraction of 6.4% with 3D fiber misalignment ($a_{11} = 0.497$, $a_{22} = 0.465$, $a_{33} = 0.038$, $a_{12} = -0.09$, $a_{13} = -0.02$, $a_{23} = 0.00$), (b) fiber aspect ratio of 29.05 and volume fraction of 15.2% with 3D fiber misalignment ($a_{11} = 0.61$, $a_{22} = 0.38$, $a_{33} = 0.01$, $a_{12} = -0.02$, $a_{13} = -0.01$, $a_{23} = 0.01$).

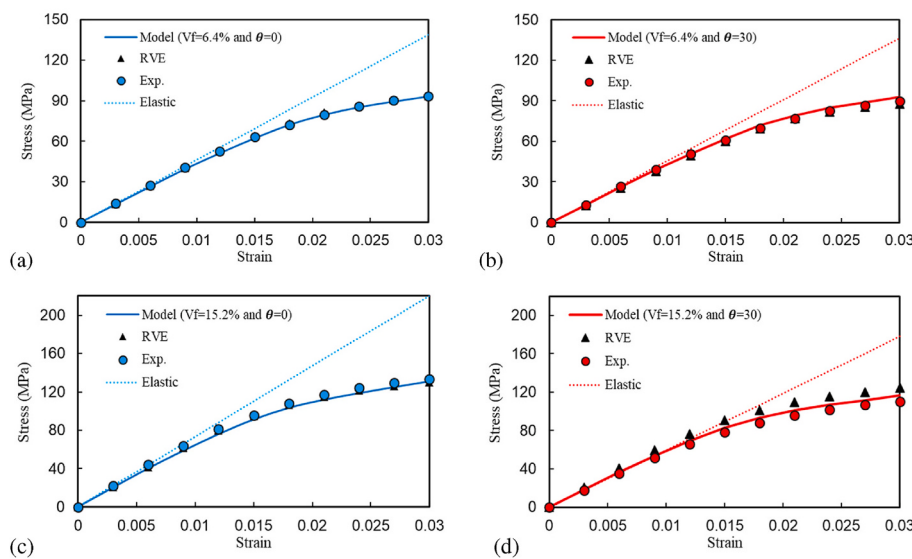


Fig. 22. The stress-strain response of glass/polyamide-6 SFRCs under tensile loading conditions with different samples; (a) fiber volume fraction 6.4% with 0-degree orientation, (b) fiber volume fraction 6.4% with 30-degree orientation, (c) fiber volume fraction 15.2% with 0-degree orientation, (d) fiber volume fraction 15.2% with 30-degree orientation.

homogenized response of the SFRCs in the continuum domain. It was illustrated that Hill's plasticity model calibrated with the unit cell analysis can efficiently capture the nonlinear mechanical response of aligned SFRCs and it can also eliminate the requirement for the microstructural analysis in each loading step. Furthermore, an easy-to-use orientation averaging framework was suggested to take into account the effects of fiber misalignment without the necessity to implement different analytical solutions. Using a multi-step homogenization strategy, the effects of core/shell were considered. The validity and effectiveness of the proposed multi-scale strategy were indicated using different RVE-generated data for complex microstructures and experimental measurements. Further investigation can be performed to add the effects of other non-linear effects such as presence of damage mechanism to the model. Moreover, the study can be extended to consider the influence of strain rate and temperatures.

Author statement

Hossein Ahmadi: Conceptualization, Methodology, Software, Formal analysis, Investigation, Visualization, Writing - Original Draft. **Mohammad Hajikazemi:** Supervision, Conceptualization, Writing - Review & Editing, **Wim Van Paepengem:** Supervision, Conceptualization, Funding acquisition, Writing - Review & Editing.

Declaration of competing interest

The authors declare that they have no known competing financial interests or personal relationships that could have appeared to influence the work reported in this paper.

Data availability

Data will be made available on request.

Acknowledgments

The work leading to this publication has been funded by the ICON project "ProPeL", which fits in the MacroModelMat (M3) research program, coordinated by Siemens (Siemens Digital Industries Software, Belgium), and funded by SIM (Strategic Initiative Materials in Flanders) and VLAIO (Flemish government agency Flanders Innovation &

Entrepreneurship). M. Hajikazemi acknowledges the financial support of Fonds voor Wetenschappelijk Onderzoek (Grant No. 1202522N). The work of M. Hajikazemi forms part of the research programme of DPI, project 812T17.

References

- [1] Xu H, Kuczynska M, Schafet N, Welschinger F, Hohe J. Modeling the anisotropic temperature-dependent viscoplastic deformation behavior of short fiber reinforced thermoplastics. Compos Sci Technol 2021;213:108958.
- [2] Hanhan I, Sangid MD. Damage propagation in short fiber thermoplastic composites analyzed through coupled 3D experiments and simulations. Compos B Eng 2021; 218:108931.
- [3] Belmonte E, De Monte M, Hoffmann C-J, Quaresimin M. Damage mechanisms in a short glass fiber reinforced polyamide under fatigue loading. Int J Fatig 2017;94: 145–57.
- [4] Zhang Y-Y, Sun Z, Li Y-Q, Huang P, Chen Q, Fu S-Y. Tensile creep behavior of short-carbon-fiber reinforced polyetherimide composites. Compos B Eng 2021;212: 108717.
- [5] Pei S, Wang K, Li J, Li Y, Zeng D, Su X, et al. Mechanical properties prediction of injection molded short/long carbon fiber reinforced polymer composites using micro X-ray computed tomography. Compos Appl Sci Manuf 2020;130:105732.
- [6] Sliseris J, Yan L, Kasal B. Numerical modelling of flax short fibre reinforced and flax fibre fabric reinforced polymer composites. Compos B Eng 2016;89:143–54.
- [7] Ahmadi H, Jahanshahi M, Khoei AR, Bordas S. Mechanical behavior of multilayer graphene reinforced epoxy nano-composites via a hierarchical multi-scale technique. Carbon Trends 2021;4:100048.
- [8] Mehdi Pour H, Camanho PP, Belingardi G. Elasto-plastic constitutive equations for short fiber reinforced polymers. Compos B Eng 2019;165:199–214.
- [9] Gusev AA. Finite element estimates of viscoelastic stiffness of short glass fiber reinforced composites. Compos Struct 2017;171:53–62.
- [10] Horst JJ, Salienko NV, Spoormaker JL. Fibre-matrix debonding stress analysis for short fibre-reinforced materials with matrix plasticity, finite element modelling and experimental verification. Compos Appl Sci Manuf 1998;29(5):525–31.
- [11] Mirkhalaf SM, Eggels EH, van Beurden TJH, Larsson F, Fagerström M. A finite element based orientation averaging method for predicting elastic properties of short fiber reinforced composites. Compos B Eng 2020;202:108388.
- [12] Zhong Y, Liu P, Pei Q, Sorkin V, Louis Commillus A, Su Z, et al. Elastic properties of injection molded short glass fiber reinforced thermoplastic composites. Compos Struct 2020;254:112850.
- [13] Babu KP, Mohite PM, Upadhyay CS. Development of an RVE and its stiffness predictions based on mathematical homogenization theory for short fibre composites. Int J Solid Struct 2018;130–131:80–104.
- [14] Islam M, Tudry GJ, Picu CR. Microstructure modeling of random composites with cylindrical inclusions having high volume fraction and broad aspect ratio distribution. Comput Mater Sci 2016;125:309–18.
- [15] Tang H, Chen H, Sun Q, Chen Z, Yan W. Experimental and computational analysis of structure-property relationship in carbon fiber reinforced polymer composites fabricated by selective laser sintering. Compos B Eng 2021;204:108499.
- [16] Naili C, Doghri I, Kanit T, Sukiman MS, Aissa-Berries A, Imad A. Short fiber reinforced composites: unbiased full-field evaluation of various homogenization methods in elasticity. Compos Sci Technol 2020;187:107942.

- [17] Wang L, Nygren G, Karkkainen RL, Yang Q. A multiscale approach for virtual testing of highly aligned short carbon fiber composites. *Compos Struct* 2019;230:111462.
- [18] Hanhan I, Agyei RF, Xiao X, Sangid MD. Predicting microstructural void nucleation in discontinuous fiber composites through coupled in-situ X-ray tomography experiments and simulations. *Sci Rep* 2020;10(1):3564.
- [19] Belmonte E, De Monte M, Riedel T, Quaresimin M. Local microstructure and stress distributions at the crack initiation site in a short fiber reinforced polyamide under fatigue loading. *Polym Test* 2016;54:250–9.
- [20] Ahmadi H, Hajikazemi M, Rashidinejad E, Sinchuk Y, Van Paepegem W. A hierarchical multi-scale analytical approach for predicting the elastic behavior of short fiber reinforced polymers under triaxial and flexural loading conditions. *Compos Sci Technol* 2022;225:109452.
- [21] Hine PJ, Rudolf Lusti H, Gusev AA. Numerical simulation of the effects of volume fraction, aspect ratio and fibre length distribution on the elastic and thermoelastic properties of short fibre composites. *Compos Sci Technol* 2002;62(10):1445–53.
- [22] Bargmann S, Klusemann B, Markmann J, Schnabel JE, Schneider K, Soysalcan C, et al. Generation of 3D representative volume elements for heterogeneous materials: a review. *Prog Mater Sci* 2018;96:322–84.
- [23] De Monte M, Moosbrugger E, Quaresimin M. Influence of temperature and thickness on the off-axis behaviour of short glass fibre reinforced polyamide 6.6 – quasi-static loading. *Compos Appl Sci Manuf* 2010;41(7):859–71.
- [24] Holmström PH, Hopperstad OS, Clausen AH. Anisotropic tensile behaviour of short glass-fibre reinforced polyamide-6. *Composites Part C: Open Access* 2020;2:100019.
- [25] Lionetto F, Montagna F, Natali D, De Pascalis F, Nacucchi M, Caretto F, et al. Correlation between elastic properties and morphology in short fiber composites by X-ray computed micro-tomography. *Compos Appl Sci Manuf* 2021;140:106169.
- [26] Breuer K, Stommel M. RVE modelling of short fiber reinforced thermoplastics with discrete fiber orientation and fiber length distribution. *SN Appl Sci* 2019;2(1):91.
- [27] Huang Z-M, Zhang C-C, Xue Y-D. Stiffness prediction of short fiber reinforced composites. *Int J Mech Sci* 2019;161–162:105068.
- [28] Rashidinejad E, Ahmadi H, Hajikazemi M, Van Paepegem W. Modeling of geometric configuration and fiber interactions in short fiber reinforced composites via new modified Eshelby tensors and enhanced mean-field homogenization. *Mech Mater* 2021;104059.
- [29] Mirkhalaf SM, van Beurden TJH, Ekh M, Larsson F, Fagerström M. An FE-based orientation averaging model for elasto-plastic behavior of short fiber composites. *Int J Mech Sci* 2022;219:107097.
- [30] Jain A, Abdin Y, Van Paepegem W, Verpoest I, Lomov SV. Effective anisotropic stiffness of inclusions with debonded interface for Eshelby-based models. *Compos Struct* 2015;131:692–706.
- [31] Brassart L, Doghri I, Delannay L. Homogenization of elasto-plastic composites coupled with a nonlinear finite element analysis of the equivalent inclusion problem. *Int J Solid Struct* 2010;47(5):716–29.
- [32] Ogierman W. A new model for time-efficient analysis of nonlinear composites with arbitrary orientation distribution of fibres. *Compos Struct* 2021;273:114310.
- [33] Tucker III CL, Liang E. Stiffness predictions for unidirectional short-fiber composites: review and evaluation. *Compos Sci Technol* 1999;59(5):655–71.
- [34] Hill R. A theory of the yielding and plastic flow of anisotropic metals. *Proc R Soc London, A* 1948;193(1033):281–97.
- [35] Barlat F, Lian K. Plastic behavior and stretchability of sheet metals. Part I: a yield function for orthotropic sheets under plane stress conditions. *Int J Plast* 1989;5(1):51–66.
- [36] Hill R. Constitutive modelling of orthotropic plasticity in sheet metals. *J Mech Phys Solid* 1990;38(3):405–17.
- [37] Barlat F, Aretz H, Yoon JW, Karabin ME, Brem JC, Dick RE. Linear transformation-based anisotropic yield functions. *Int J Plast* 2005;21(5):1009–39.
- [38] Cazacu O, Plunkett B, Barlat F. Orthotropic yield criterion for hexagonal closed packed metals. *Int J Plast* 2006;22(7):1171–94.
- [39] Wang X, Guan Z, Du S, Han G, Li Z. An accurate and easy to implement method for predicting matrix crack and plasticity of composites with an efficient search algorithm for LaRC05 criterion. *Compos Appl Sci Manuf* 2020;131:105808.
- [40] Amiri-Rad A, Pastukhov LV, Govaert LE, van Dommelen JAW. An anisotropic viscoelastic-viscoplastic model for short-fiber composites. *Mech Mater* 2019;137:103141.
- [41] Amiri-Rad A, Wismans M, Pastukhov LV, Govaert LE, van Dommelen JAW. Constitutive modeling of injection-molded short-fiber composites: characterization and model application. *J Appl Polym Sci* 2020;137(41):49248.
- [42] Selmi A, Doghri I, Adam L. Micromechanical simulations of biaxial yield, hardening and plastic flow in short glass fiber reinforced polyamide. *Int J Mech Sci* 2011;53(9):696–706.
- [43] Kamoun S, Doghri I, Adam L, Robert G, Delannay L. First pseudo-grain failure model for inelastic composites with misaligned short fibers. *Compos Appl Sci Manuf* 2011;42(12):1892–902.
- [44] Jain A, Lomov SV, Abdin Y, Verpoest I, Van Paepegem W. Pseudo-grain discretization and full Mori-Tanaka formulation for random heterogeneous media: predictive abilities for stresses in individual inclusions and the matrix. *Compos Sci Technol* 2013;87:86–93.
- [45] Doghri I, Tiné L. Micromechanical modeling and computation of elasto-plastic materials reinforced with distributed-orientation fibers. *Int J Plast* 2005;21(10):1919–40.
- [46] Kamoun S, Doghri I, Brassart L, Delannay L. Micromechanical modeling of the progressive failure in short glass-fiber reinforced thermoplastics – first Pseudo-Grain Damage model. *Compos Appl Sci Manuf* 2015;73:166–75.
- [47] Tian W, Qi L, Su C, Liang J, Zhou J. Numerical evaluation on mechanical properties of short-fiber-reinforced metal matrix composites: two-step mean-field homogenization procedure. *Compos Struct* 2016;139:96–103.
- [48] Pierard O, Fribel C, Doghri I. Mean-field homogenization of multi-phase thermo-elastic composites: a general framework and its validation. *Compos Sci Technol* 2004;64(10):1587–603.
- [49] Tian W, Qi L, Su C, Zhou J, Jing Z. Numerical simulation on elastic properties of short-fiber-reinforced metal matrix composites: effect of fiber orientation. *Compos Struct* 2016;152:408–17.
- [50] Pietrogrande R, Carraro PA, De Monte M, Quaresimin M. A novel pseudo-grain approach for the estimation of the elastic stress distributions within the matrix of short fiber-reinforced polymers. *Compos B Eng* 2018;150:115–23.
- [51] Ahmadi H, Hajikazemi M, Van Paepegem W. A computational study about the effects of ply cracking and delamination on the stiffness reduction of damaged lamina and laminate. *Int J Damage Mech* 2022;31(3):325–47.
- [52] Garoz D, Gilabert FA, Sevenois RDB, Spronk SWF, Van Paepegem W. Consistent application of periodic boundary conditions in implicit and explicit finite element simulations of damage in composites. *Compos B Eng* 2019;168:254–66.
- [53] Advani SG, III CLT. The use of tensors to describe and predict fiber orientation in short fiber composites. *J Rheol* 1987;31(8):751–84.
- [54] Notta-Cuvier D, Lauro F, Bennani B, Balieu R. Damage of short-fibre reinforced materials with anisotropy induced by complex fibres orientations. *Mech Mater* 2014;68:193–206.
- [55] Camacho CW, Tucker III CL, Yalvaç S, McGee RL. Stiffness and thermal expansion predictions for hybrid short fiber composites. *Polym Compos* 1990;11(4):229–39.
- [56] Doghri I, Tiné L. Micromechanics of inelastic composites with misaligned inclusions: numerical treatment of orientation. *Comput Methods Appl Mech Eng* 2006;195(13):1387–406.
- [57] Doghri I, Brassart L, Adam L, Gérard JS. A second-moment incremental formulation for the mean-field homogenization of elasto-plastic composites. *Int J Plast* 2011;27(3):352–71.
- [58] Digimat A. Software for the linear and nonlinear multi-scale modeling of heterogeneous materials. Belgium: e-Xstream Engineering; Louvain-la-Neuve; 2011.
- [59] Advani SG, Tucker III CL. Closure approximations for three-dimensional structure tensors. *J Rheol* 1990;34(3):367–86.